Obtaining far-field spherical directivities of guitar amplifiers from arbitrarily shaped arrays using the Helmholtz equation least-squares method

Samuel David Bellows and Timothy W. Leishman

179th Meeting of the Acoustical Society of America

Acoustics Virtually Everywhere

7-11 December 2020

Signal Processing in Acoustics: Paper 5aSPb3

Obtaining far-field spherical directivities of guitar amplifiers from arbitrarily shaped arrays using the Helmholtz equation least-squares method

Samuel David Bellows and Timothy W. Leishman
Department of Physics and Astronomy, Brigham Young University, Provo, UT, 84602;
samuel.bellows11@gmail.com; twleishman@byu.edu

Commonly, directivities of sound sources are measured using surrounding spherical arrays. However, in some cases, such as when measurement hardware is limited, or when an array shape would ideally conform to the radiating object's geometry, obtaining spherical far-field directivities using an arbitrarily shaped array could be useful. This work illustrates how the Helmholtz equation least-squares method applies to accomplish this task. Both numerical models and the measured directivities of various guitar amplifiers validate the technique.

1. INTRODUCTION

Directivity measurements describe the spatial dependence of free radiated pressure fields, making them essential tools for characterizing sound sources. Researchers and practitioners have utilized various approaches for measuring directivities, but most methods currently involve constant-radius polar or spherical sampling, typically designed or assumed to be in the source far fields. The AES standard for measuring loudspeaker directivities specifies either 10° or 5° spherical resolution in the polar and azimuthal angles, leading to 614 or 2,522 unique sampling positions, respectively.[1] File structures such as the common loudspeaker format (CLF)[2] or EASE GLL[3] facilitate the sharing of the spherical data with support for various bandwidths, including narrowband or 1/1 or 1/3-octave bands. Figure 1 shows a directivity measurement array with microphones spaced at 5° in the polar angle. Full spherical data results by rotating the sound source azimuthally using a computer-controlled system. Recently, specialized transfer function techniques have allowed the 5° resolution standard to be applied to live sources such as musical instruments and speech,[4,5] with the resulting data being freely available in an archival database.[6]

While measuring directivities with spherical arrays is a straightforward process, there are several potential advantages to using arbitrarily shaped arrays, including those conforming more closely to radiators' geometries. For loudspeakers, this allows enhanced vibro-acoustic analysis using inverse methods such as near-field acoustical holography (NAH),[7] inverse boundary element method (I-BEM),[8] or the Helmholtz equation least-squares (HELS) method[9] to study cone velocity, cone breakup, and other characteristics. Near-field measurements also allow increased signal-to-noise ratios and the potential to make assessments in smaller measurement rooms or other nonideal environments. Arrays with relatively simple geometries
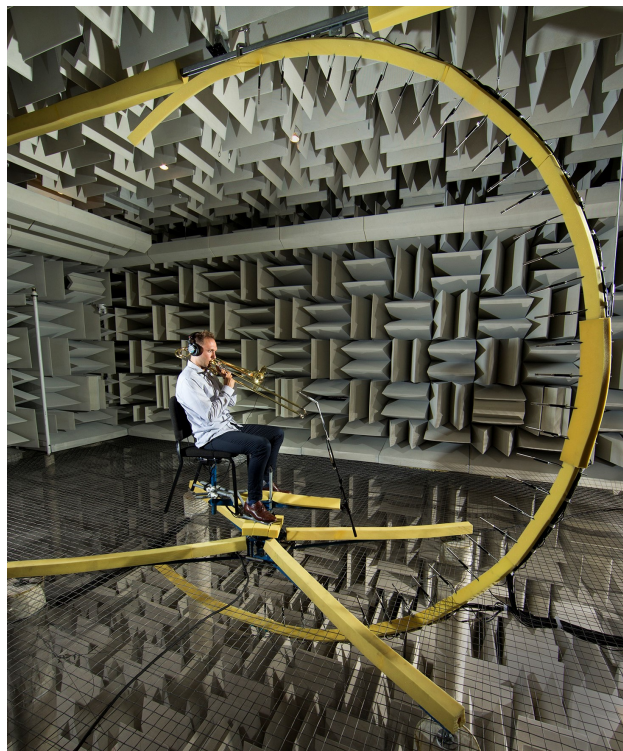
Figure 1: A microphone array used in measuring spherical directivities of musical instruments and speech. The array has 5° resolution in the polar angle. A full spherical directivity follows by rotating the musician or talker in 5° azimuthal steps and using a transfer function technique to address repetition variations.

permit directivity measurements without highly specialized apparatuses. While the underlying principles and techniques necessary for using arbitrarily shaped arrays to measure far-field directivities have been available for decades,[10] they remain relatively obscure for the measurement of loudspeakers. This work illustrates how one may obtain reliable far-field spherical directivities from sampling using arbitrarily shaped arrays by measuring several guitar amplifiers' directivities. The approach proceeds from the HELS method, and the results include both numerical and experimental validations.

2. FORMULATION

A. HELS METHOD

The exterior pressure solution to the Helmholtz equation in spherical coordinates is[7]

$$p(r, \theta, \phi, k) = \sum_{n=0}^{\infty} \sum_{m=-n}^{n} c_n^m(k) h_n^{(2)}(kr) Y_n^m(\theta, \phi), \tag{1}$$

where $p(r, \theta, \phi, k)$ is the pressure, $h_n^{(2)}(kr)$ are the spherical Hankel functions of the second kind of order n, $Y_n^m(\theta, \phi)$ are the spherical harmonics of degree n and order m,[11] and $c_n^m(k)$ are the pressure expansion coefficients. To estimate the $c_n^m(k)$, one may employ the HELS method, wherein Q measurements of the pressure appear as linear combinations of the selected basis functions $\Psi(\mathbf{r}, k)$, which, in spherical coordinates, are the products of spherical Hankel functions and spherical harmonics:

$$\Psi_n^m(r, \theta, \phi, k) = h_n^{(2)}(kr) Y_n^m(\theta, \phi). \tag{2}$$

By considering only eigenfunctions up to a maximal expansion degree N, the system of equations takes the matrix form

$$\mathbf{p} = \mathbf{\Psi} \mathbf{c} + \mathbf{e}, \tag{3}$$

where

$$\mathbf{p} = \begin{bmatrix} p(\mathbf{r}_1, k) & p(\mathbf{r}_2, k) & \cdots & p(\mathbf{r}_Q, k) \end{bmatrix}^T, \tag{4}$$

$$\mathbf{c} = \begin{bmatrix} c_0^0(k) & c_1^{-1}(k) & \cdots & c_N^N(k) \end{bmatrix}^T, \tag{5}$$

$$\mathbf{\Psi} = \begin{bmatrix} \Psi_0^0(\mathbf{r}_1, k) & \Psi_1^{-1}(\mathbf{r}_1, k) & \cdots & \Psi_N^N(\mathbf{r}_1, k) \\ \Psi_0^0(\mathbf{r}_2, k) & \Psi_1^{-1}(\mathbf{r}_2, k) & \cdots & \Psi_N^N(\mathbf{r}_2, k) \\ \vdots & \vdots & \ddots & \vdots \\ \Psi_0^0(\mathbf{r}_Q, k) & \Psi_1^{-1}(\mathbf{r}_Q, k) & \cdots & \Psi_N^N(\mathbf{r}_Q, k) \end{bmatrix}, \tag{6}$$

$\mathbf{e}$ is a column vector representing the least-squares errors, and $\mathbf{r}_q$, with $q = 1, 2, ..., Q$, represent the Q arbitrary sampling positions. If the number of positions exceeds the number of required coefficients, the least-squares solution to the overdetermined system follows as

$$\mathbf{c} = \mathbf{\Psi}^\dagger \mathbf{p}, \tag{7}$$

where the pseudo-inverse $\mathbf{\Psi}^\dagger$ is

$$\mathbf{\Psi}^\dagger = (\mathbf{\Psi}^H \mathbf{\Psi})^{-1} \mathbf{\Psi}^H. \tag{8}$$

For the present work, a regularized least-squares fit was sometimes beneficial, particularly when sparse sampling densities occurred in particular spatial regions. The Tikhonov regularization (ridge regression) was well suited, in which the regularized pseudo-inverse $\boldsymbol{\Psi}_\lambda^\dagger$ is[12]

$$\boldsymbol{\Psi}_\lambda^\dagger = (\boldsymbol{\Psi}^H \boldsymbol{\Psi} + \lambda \mathbf{I})^{-1} \boldsymbol{\Psi}^H, \tag{9}$$

where $\lambda > 0$ is the regularization parameter, determined ad hoc.

B. FAR-FIELD DIRECTIVITY PATTERN

By applying the large-argument relation of the spherical Hankel functions,

$$h_n^{(2)}(kr) \approx i^{n+1} \frac{e^{-ikr}}{kr}, \qquad kr >> 1, \tag{10}$$

the far-field pressure becomes

$$p(r, \theta, \phi, k) \approx \frac{e^{-ikr}}{kr} \sum_{n=0}^{\infty} \sum_{m=-n}^{n} c_n^m(k) i^{n+1} Y_n^m(\theta, \phi), \tag{11}$$

comprising a spherical wave with the unnormalized far-field directivity function

$$\tilde{D}_\infty(\theta, \phi, k) = \sum_{n=0}^{\infty} \sum_{m=-n}^{n} c_n^m(k) i^{n+1} Y_n^m(\theta, \phi). \tag{12}$$

Thus, to compute the far-field spherical directivity, one first measures the acoustic pressure at Q distinct near-field positions. Next, the HELS method produces the expansion coefficients $c_n^m(k)$ using an overdetermined system of equations. Finally, the spherical harmonic expansion of Eq. (12) represents the far-field directivity pattern.

3. NUMERICAL RESULTS

A. ARRAY SAMPLING SCHEMES

A simple loudspeaker model provided a convenient means to numerically validate the method for four distinct near-field arrays, each with plausible geometries. Figure 2 shows the selected arrays surrounding the model. The first is a spherical array with 10° resolution in the polar and azimuthal angles and 614 unique sampling positions, which coincides with the AES standard. The second is a prolate-spheroidal grid based on a sampling resolution similar to that of the spherical array, having the same number of positions. The third is a cylindrical array with a flat top and bottom and 602 unique sampling positions. The final array comprises a rectangular prism (cuboid), also with 602 unique sampling positions. The number of sampling positions for each array is approximately equal but constrained by their different shapes.

The array's dimensions allowed them to nearly graze the 40 cm × 25 cm × 15 cm loudspeaker model with the nearest microphones of the array at 10% of its maximum extent. Finally, a far-field spherical reference array with 5 m radius and 5° resolution validated the HELS method's spherical directivities. Table 1 reports the smallest, mean, and largest radial positions of each near-field sampling scheme as measured from the origin.
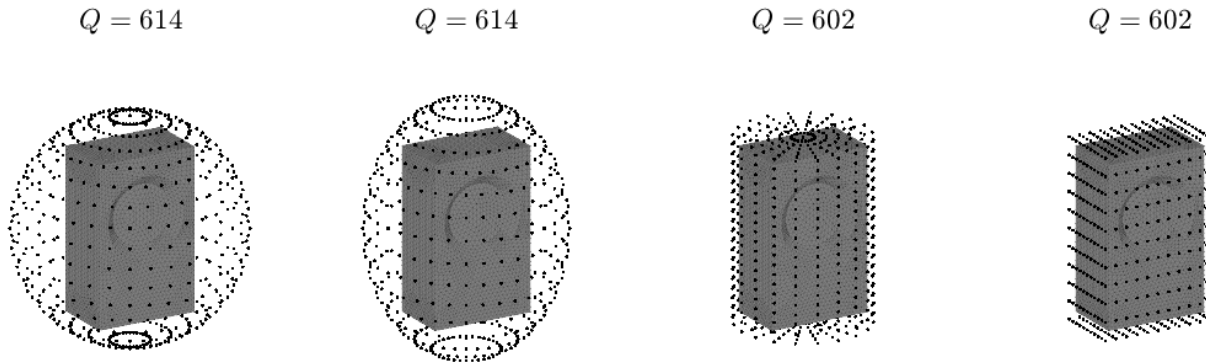
Figure 2: Spherical, spheroidal, cylindrical, and rectangular prism arrays used in the numerical experiments. The number of unique sampling positions appears above each array.
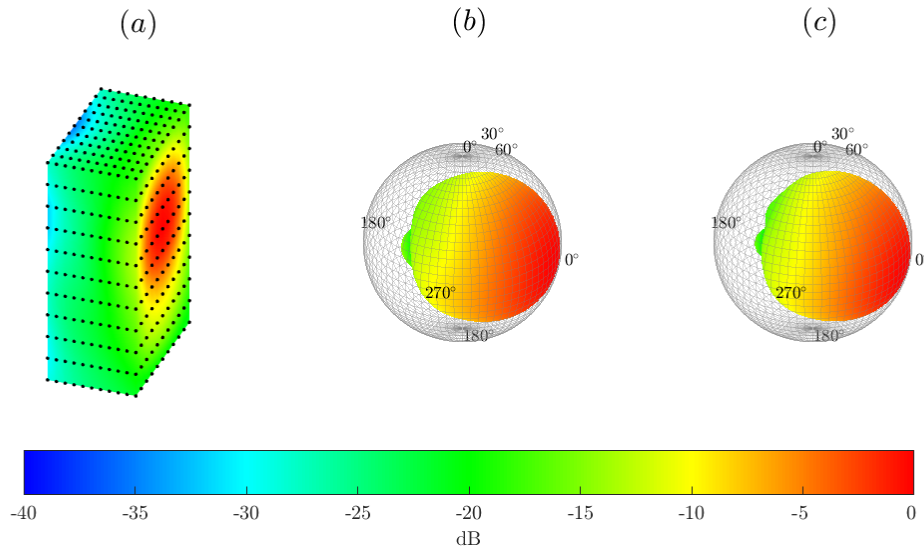
B. BEM RESULTS

The boundary element method (BEM) produced the pressure at each sampling position of each array over a 100 Hz to 5 kHz bandwidth for the numerical experiments. From the calculated pressures, the HELS method estimated the expansion coefficients $c_n^m(k)$. Finally, propagating the pressure results to the far-field enabled the evaluation of the directivity through a 5° degree polar and azimuthal sampling scheme and subsequent comparison to the reference spherical array results.

Figure 3 shows the results for the rectangular prism array at 1 kHz. Figure 3a gives the relative sound pressure level on the array surface, Fig. 3b shows the estimated far-field spherical directivity using a degree $N = 6$ expansion, and Fig. 3c shows the reference far-field directivity without any expansion. All plots appear on a normalized 40 dB scale relative to the maximum pressure. The far-field patterns are very similar, albeit with some discrepancies behind the loudspeaker, which appear in the balloons' green-colored regions. This trend was consistent for various numerical experiments, as the regions that were many dB down from the maximum were challenging to estimate with high accuracy.

An essential part of the far-field estimation process is the selection of the expansion degree N. The choice is critical because it helps minimize the error of the associated directivity pattern. Figure 4 shows the results for the rectangular prism array at 2 kHz and compares the effects of various expansion degrees. When the degree is too small, such as $N = 1$ in Fig. 4a, the pattern does not accurately represent the measured pressure because of excess bias caused by too few degrees of freedom in the eigenfunction expansion. As the degree increases, the bias reduces, and the results agree better with the measured pressure, such as with the $N = 6$ balloon shown in Fig. 4c. However, if the degree becomes too high, such as for the $N = 15$ balloon in Fig. 4c, it produces too much variance, and the overfitting causes the model to deviate from the measured pressure. The degree $N = 6$ balloon was the best fit for this particular frequency. Its features are

Table 1: Sampling scheme radii for the various near-field arrays.

Array Shape	Smallest Radial Position (m)	Mean Radial Position (m)	Largest Radial Position (m)
Spherical	0.27	0.27	0.27
Spheroidal	0.24	0.27	0.31
Cylinder	0.16	0.22	0.27
Prism	0.08	0.20	0.27

Figure 3: *The BEM results for the rectangular prism array at 1 kHz. (a) Evaluated pressure on the prism array surface. (b) Estimated far-field directivity using the HELS method. (c) Reference far-field array directivity.*

similar to those of the measured far-field balloon, but it still has some notable differences. In practice, as one does not know the far-field pattern beforehand, it is necessary to monitor the expansion's degree carefully. A model degree $N = kd$, where d is the maximum dimension of the radiating object, seemed to give a reasonable initial estimate. This prediction approximately represented the maximum degree of the spherical eigenfunctions that did not rapidly evanesce before reaching the far-field.[7]

## C.   NUMERICAL EXPERIMENTAL ERRORS

One way to establish the frequency-dependent error between the directivity results of the various array types and the reference far-field pattern is to compute the spherically area-weighted deviation (AWD),[13]

$$\sigma^2_{AWD} = \sum_i w_i \left[\frac{|\tilde{D}(\theta, \phi, k)| - |\tilde{D}_{ref}(\theta, \phi, k)|}{|\tilde{D}_{ref}(\theta, \phi, k)|} \right]^2, \tag{13}$$

where $\tilde{D}$ represents the normalized directivity, $\tilde{D}_{ref}$ is the normalized reference directivity, and w_i are Chebyshev quadrature weights for the 5° sampling.[14] On a logarithmic scale, the deviation becomes

$$L_{AWD} = 10 \log_{10}(1 + \sigma^2_{AWD}). \tag{14}$$

For each array type, the best estimations of the far-field directivity pattern at each frequency resulted from increasing the expansion degree N to select the lowest error between it and the known far-field pattern. While this is not generally possible under experimental conditions, since the far-field pattern is unknown, this procedure provided the best-case scenario for a given array at a given frequency. Figure 5 compares selected directivity balloons from the arrays at 100 Hz, 2 kHz, 3 kHz, and 5 kHz. The top figure row shows the far-field spherical reference array results, while the subsequent rows show the propagated results from the spheroidal, cylindrical, and rectangular prism arrays. When the directivity patterns are simple and
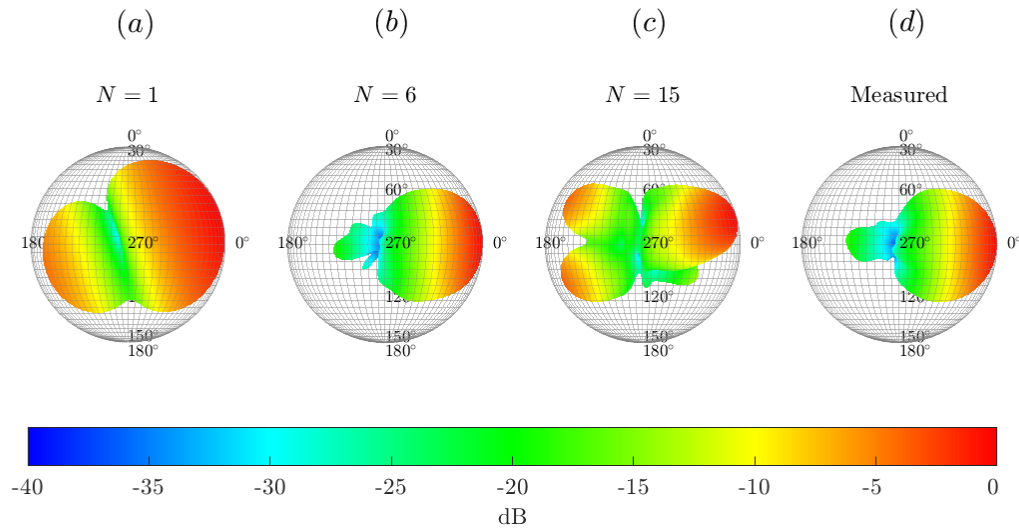
Figure 4: Illustration of the bias-variance trade-offs that arise when estimating far-field directivity patterns from near-field sampled pressures. (a) Far-field directivity based on degree $N = 1$ expansion. (b) Far-field directivity based on degree $N = 6$ expansion. (c) Far-field directivity based on degree $N = 15$ expansion. (d) Far-field reference directivity.

nearly omnidirectional at low frequencies, they all show good agreement. However, as frequency increases, the patterns' deviations become more apparent, particularly for the cylindrical and prism arrays.

As shown in Fig. 6, the errors between all array results and the reference pattern are consistently small at low frequencies across the sampling schemes. However, as frequency increases, the varied array performances become more evident. In particular, the near-field spherical array performed best, followed in order by the spheroidal, cylindrical, and rectangular prism arrays. These trends suggest that the closer a near-field array is to a spherical geometry, the better it enables pressure propagation to the far field to match the spherical far-field directivity pattern. One may note that the spherical and spheroidal arrays had an additional twelve sampling positions; however, since this represents only about 2% of the total number of sampling positions for the cylindrical and prism arrays, the related effect is presumably negligible. The errors begin to increase above about 2 kHz for the given sampling positions of all arrays, which corresponds to a value of $kd \approx 9$. However, the spheroidal and spherical arrays' deviations remain well below 0.1 dB for all frequencies below 5 kHz.

4. EXPERIMENTAL RESULTS

The experimental validation included four guitar amplifiers' measured directivities: Fender Princeton Reverb, Fender Twin Reverb, Fender Deluxe Reverb, and VOX AC30. The experimental array shown in Fig. 7 consisted of 14 microphones arranged for cylindrical scanning. One near-field microphone produced a reference signal for computing frequency response functions, and one far-field microphone produced a signal for validating propagated results in the transverse plane. The entire cylindrical sampling surface developed gradually as the amplifier rotated in 5° degree azimuthal increments, resulting in 937 unique sampling positions on the array surface and 72 unique sampling positions for reference in the transverse plane. In the initial configuration shown in Fig. 7, the microphone arrangement below the guitar amplifier created
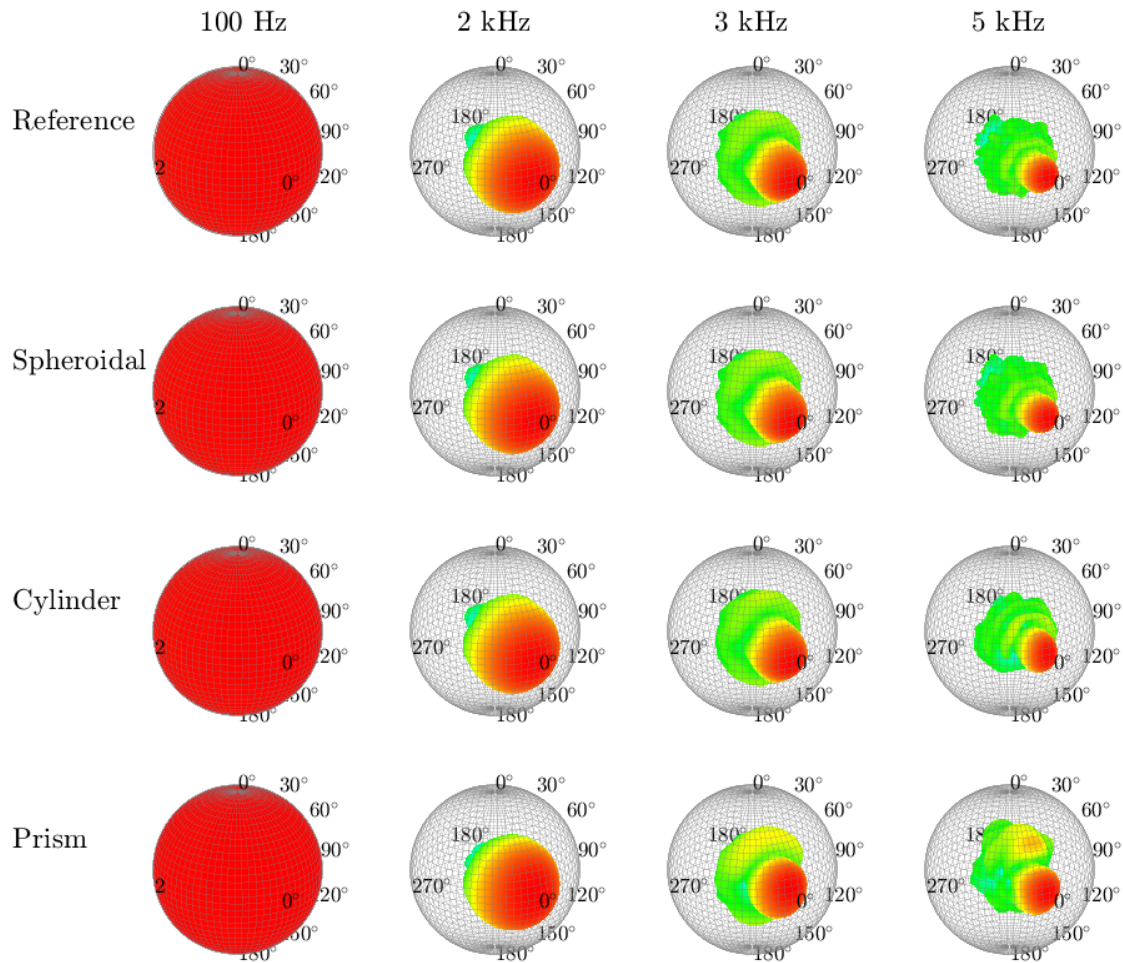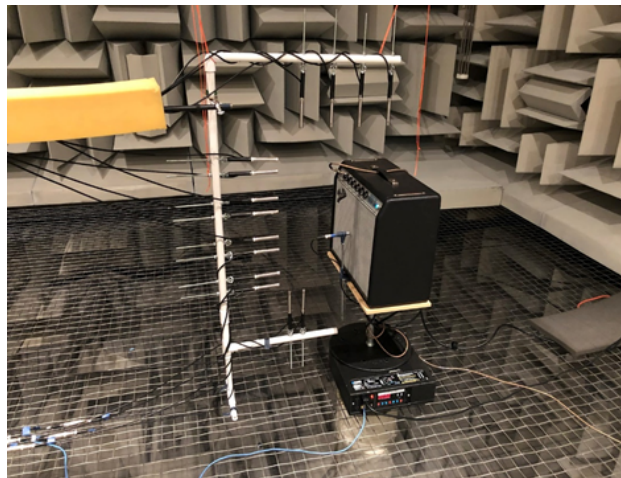
Figure 5: Selected results at 100 Hz, 2 kHz, 3 kHz, and 5 kHz for the far-field reference array in comparison to the spheroidal, cylindrical, and rectangular prism arrays.
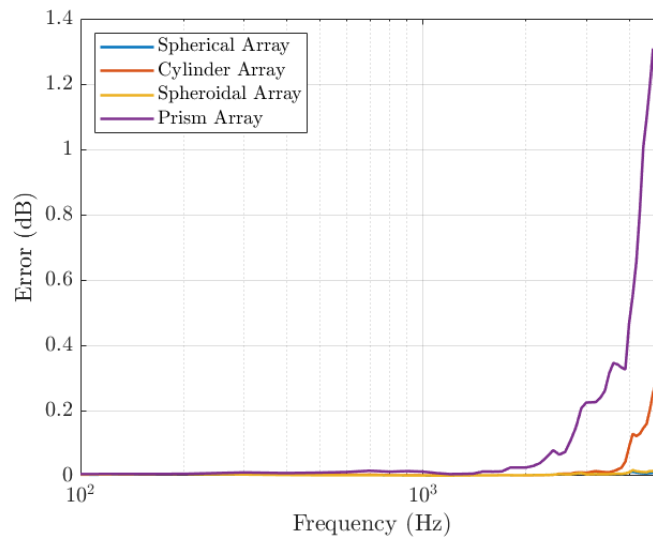
*Figure 6: The AWD levels for the BEM experiments involving different array types.*

Figure 7: Experimental validation setup for the Fender Princeton Reverb amplifier, showing the 14 microphone near-field array. Of note is the gap in the microphone placement near the bottom of the guitar amplifier.

a sparsely sampled region that allowed the investigation of associated effects. For later measurements, the bottom microphone nearest to the guitar amplifier shifted closer to it.

A. PRINCETON REVERB

Figure 8 shows directivity results for the Fender Princeton Reverb at 100 Hz based on a degree $N = 3$ expansion. Because the amplifier has an open back, the radiation pattern at low frequencies has dipole-like characteristics, evident in both the estimated far-field spherical directivity of Fig. 8a and the transverse-plane polar directivity of Fig. 8b. The measured and estimated far-field transverse directivities in Fig. 8b show good agreement.

As frequency increased, the use of regularization helped mitigate errors due to sparse sampling. Figure 9 shows the results at 1 kHz using a degree $N = 8$ expansion. In Fig. 9b, the transverse-plane measured
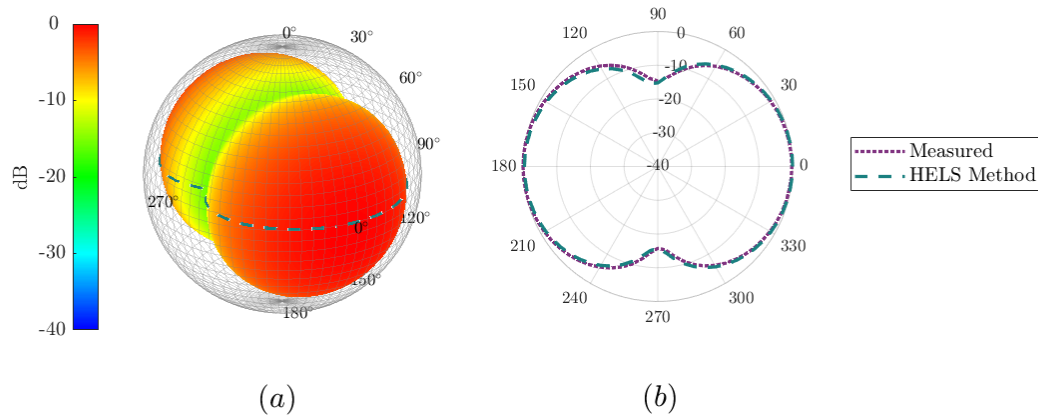
Figure 8: Directivity results for the Fender Princeton Reverb amplifier at 100 Hz. (a) Estimated spherical far-field directivity pattern from the HELS method based on degree $N = 3$ expansion, with the transverse polar directivity overlaid as a green dashed line. (b) Measured transverse far-field directivity and estimated transverse directivity.

and estimated directivities agree well in front of and behind the amplifier, but less so within the null regions toward the sides. Interestingly, a large lobe has formed below the guitar amplifier, despite no dominant radiation in that direction. This effect results from a lack of sampling constraints directly below the amplifier, which allows the least-squares fit to reduce the error at other array positions at the expense of higher error in the unconstrained region. Regularization mitigates this outcome by penalizing the prevailing norm of the expansion coefficients. Figure 10 shows improved directivity results for the same frequency and expansion degree but with coefficients computed using the regularized pseudo-inverse. The large lobe below the amplifier in Fig. 9a is no longer visible in Fig. 10a, whereas the main lobe caused by the true amplifier radiation remains intact. The measured and estimated transverse-plane directivities in Fig. 10b also show better general agreement, including significantly improved correspondence in the side null regions.

B.   TWIN REVERB

An array reconfiguration that better distributed the bottom microphone positions improved measurement performance and reduced the sparse sampling errors. However, because the bottom microphones were still unable to measure radiation directly beneath the amplifier, regularization remained necessary. Figure 11 shows the results for the Fender Twin Reverb at 1.5 kHz. Similar to the Princeton Reverb, the Twin Reverb is an open-back amplifier. However, unlike the Princeton Reverb, the Twin Reverb includes two front-facing loudspeaker drivers. In the directivity balloon shown in Fig. 11a, these drivers create an interesting interference pattern with three frontal lobes. The estimated far-field directivity followed from a degree-12 expansion with regularization. There is good agreement between the measured and estimated transverse far-field directivities as shown in Fig. 11b. However, within regions more than 10 dB down from the maximum, the method is less reliable.

5.   DISCUSSION

This work's numerical and experimental results indicate that estimating sound sources' far-field spherical directivities using arbitrarily shaped near-field arrays is plausible. The error curves from BEM results
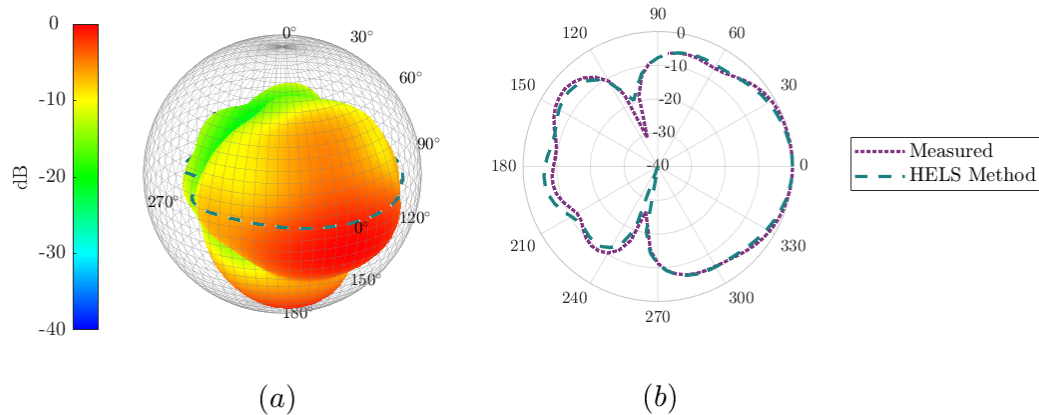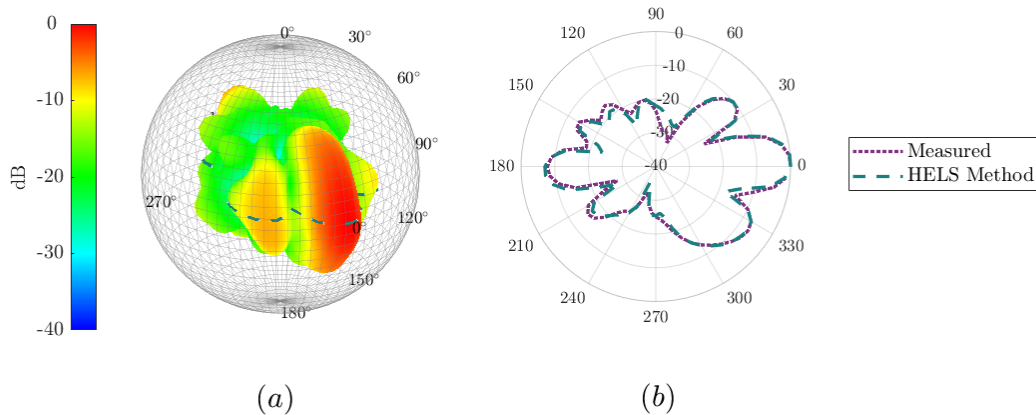
Figure 9: Directivty results for the Fender Princeton Reverb amplifier at 1 kHz without regularization. (a) Estimated spherical far-field directivity pattern based on a degree $N = 8$ expansion, with the transverse polar directivity overlaid as a green dashed line. (b) Measured transverse far-field directivity and estimated transverse directivity from the HELS method. Of note is the large lobe below the guitar amplifier shown in (a), where the sampling was sparse.

suggest that while all the tested arrays performed roughly the same at low frequencies, the more spherical arrays performed better at higher frequencies. More rigorous analysis is necessary to strengthen this observation and determine the usable bandwidths and other limitations of near-field array types for specific source shapes and dimensions. The work's BEM and experimental results showed that the method's performance began deteriorating above about 2 kHz. As frequency increased, estimation errors also increased but
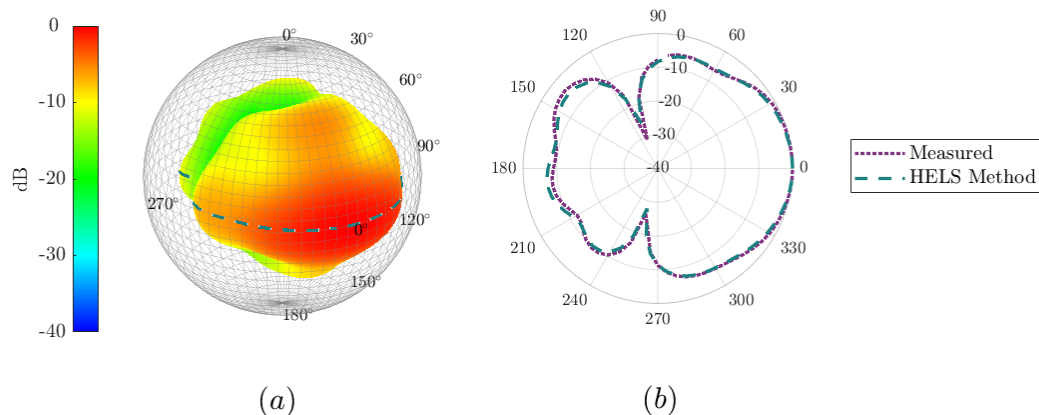
Figure 10: Directivity results for the Fender Prinecton Reverb amplifier at 1 kHz with regularization. (a) Estimated spherical far-field directivity pattern based on a degree $N = 8$ expansion, with the transverse polar directivity overlaid as a green dashed line. (b) Measured transverse far-field directivity and estimated transverse directivity from the HELS method. Regularization has removed the large bottom lobe seen in Fig. 9a and increased the agreement between the estimated and measured transverse directivities.

Figure 11: Directivity results for the Fender Twin Reverb apmplifier at 1.5 kHz. (a) Spherical far-field directivity pattern based on a degree $N = 12$ expansion and regularization, with the transverse polar directivity overlaid as a green dashed line. (b) Measured transverse far-field directivity and estimated transverse directivity from the HELS method.

were concentrated primarily in regions that were many dB down from the directivity maximum. For some applications, these errors may be negligible, provided there is an accurate estimation of the directivity in regions where the most sound energy radiates. Future evaluation metrics may benefit from weighting errors by the intensities in given directions, thus penalizing substantial radiation regions more than weaker ones. In the numerical experiments, the method tended to perform better when sampling positions were within the radiating source's near-field. Consequently, as frequency increases, it may also become desirable to utilize a hybrid approach with far-field propagators.[15] To optimize the model degree, the authors found that $N = kd$ gave a reasonable initial estimate that may benefit from further refinement. Regularization helped improve the quality of the estimated patterns, mainly when sampling was sparse.

6. CONCLUSIONS

This work has illustrated, both numerically and experimentally, how to obtain far-field spherical directivity patterns of sources using arbitrarily shaped near-field arrays and the HELS method, especially at lower frequencies. However, one must ensure that the expansion degree and regularization are sufficient to provide meaningful results. Future work could include theoretical and experimental exploration of additional sampling configurations and the validation of experimental results using a known spherical directivity instead of only a polar directivity in a single plane. This work's arrays formed specific shapes, viz., spheres, spheroids, cylinders, and rectangular prisms. It could be of interest to study randomly distributed sampling positions, although this would most likely provide more theoretical insight than practical use in future directivity measurements.

ACKNOWLEDGMENTS

REFERENCES

[1] AES56-2008 (r2014): *AES Standard on Acoustics: Sound Source Modeling: Loudspeaker Polar Radiation Measurements* (Audio Engineering Society, New York, 2015).

[2] CLF Group, "CLF: A common loudspeaker format," Syn-Aud-Con Newsl. **32**(4), 14-17 (2004).

[3] Ahnert Feistel Media Group, "GLL loudspeaker file format," (2021).
https://ease.afmg.eu/index.php/gll-loudspeaker-format.html (Last viewed February 20, 2021).

[4] K. J. Bodon, "Development, evaluation, and validation of a high-resolution directivity measurement system for played musical instruments," Master's thesis, Brigham Young University, 2016.

[5] T. W. Leishman, S. D. Bellows, C. M. Pincock, and J. K. Whiting, "High-resolution spherical directivity of live speech from a multiple-capture transfer function method," *Journal of the Acoustical Society of America*, **149**(3), pp. 1507–1523, 2021.

[6] "Directivity," Brigham Young University ScholarsArchive (2019).
https://scholarsarchive.byu.edu/directivity/ (Last viewed February 20, 2021).

[7] E. G. Williams, *Fourier Acoustics: Sound Radiation and Nearfield Acoustical Holography*. London: Academic Press, 1999.

[8] M. R. Bai, "Application of BEM (boundary element method)-based acoustic holography to radiation analysis of sound sources with arbitrarily shaped geometries," *The Journal of the Acoustical Society of America*, **92**(1), pp. 533–549, 1992.

[9] S. F. Wu, *The Helmholtz Equation Least Squares Method: For Reconstructing and Predicting Acoustic Radiation*. Springer, 2015.

[10] C. W. Horton and G. S. Innis, "The computation of far-field radiation patterns from measurements made near the source," *The Journal of the Acoustical Society of America*, **33**(7), pp. 877–880, 1961.

[11] T. M. Dunster, *NIST Handbook of Mathematical Functions*. New York: Cambridge University Press, 2010.

[12] G. Strang, *Linear Algebra and Learning from Data*. Wellesley-Cambridge Press, 2019.

[13] T. W. Leishman, S. Rollins, and H. M. Smith, "An experimental evaluation of regular polyhedron loudspeakers as omnidirectional sources of sound," *Journal of the Acoustical Society of America*, **120**(3), pp. 1411–1422, 2006.

[14] S. D. Bellows and T. W. Leishman, "Spherical harmonic expansions of high-resolution musical instrument directivities," *Proc. Mtgs. Acoust. 35, 035005*, 2018.

[15] M. Bru, "Cylinder measurement method for directivity balloons," in *Audio Engineering Society Convention 149*, Oct 2020.